PERGAMON

Electrochimica Acta 46 (2001) 1215–1222

ELECTROCHIMICA Acta

www.elsevier.nl/locate/electacta

Structural and electrochemical characterization of lithium excess and Al-doped nickel oxides synthesized by the sol–gel method

Sang Ho Park [a], Ki Soo Park [a], Yang Kook Sun [b], Kee Suk Nahm [a,*], Yun Sung Lee [c], Masaki Yoshio [c]

[a] *School of Chemical Engineering and Technology, College of Engineering, Chonbuk National University, Chonju 561-756, South Korea*

[b] *Department of Industrial Chemistry, College of Engineering, Hanyang University, Seoul 133-791, South Korea*

[c] *Department of Applied Chemistry, Saga University, 1 Honjo, Saga 840-8502, Japan*

Received 30 August 2000; received in revised form 25 October 2000

Abstract

The effects of excess lithium and aluminum doping in nickel oxide were investigated in an attempt to improve electrochemical properties of the layered $LiNiO_2$. $Li_{1+x}NiO_2$ ($x = 0$–0.02) and $LiAl_yNi_{1-y}O_2$ ($y = 0$–0.3) powders were synthesized by a sol–gel method using adipic acid as a chelating agent. The electrochemical properties of the synthesized materials were explored at room and high temperatures. Gas analysis during decomposition of gel precursors revealed that oxygen might play an important role in the synthesis of highly crystallized $LiNiO_2$. Although the electrochemical test of the Al-doped samples showed a low initial discharge capacity of about 140 mAh g^{-1}, the capacity loss with repeated cycling was very small at room temperature. Furthermore the fade in capacity of this cell at high temperature (50°C) was almost negligible. The Al-doping of the $LiNiO_2$ cathode material was very effective in improving cycle performance at high temperature due to the enhanced stability of $LiNiO_2$ structure.

Keywords: Excess lithium; Lithium nickel oxide; Sol–gel method; Aluminum doping; High temperature electrochemical properties

1. Introduction

Layered lithium metal oxides such as $LiCoO_2$ and $LiNiO_2$ have been of great interest as cathode materials for secondary lithium batteries [1–3]. Recently $LiNiO_2$ has been intensely investigated because of its comparatively low cost, large theoretical capacity (275 mAh g^{-1}), and environmental advantages over $LiCoO_2$ [4–6]. However, it still has problems, which need to be settled for the wider usage in practical lithium batteries. The discharge capacity of $LiNiO_2$ measured experimentally was certified to have about 140–150 mAh g^{-1} due to the synthesis of non-stoichiometric $LiNiO_2$ [7]. It is difficult to synthesize stoichiometric $LiNiO_2$ because of the loss of lithium from the host structure during high temperature calcination due to the high vapor pressure of lithium [3]. This leads to the formation of non-stoichiometric $[Li_{1-x}Ni_x]_{3b}[Ni_{1-x}]_{3a}[O_2]_{6c}$ structure, resulting in the low initial capacity of $LiNiO_2$ as well as capacity loss during cycling [8]. Another typical problem is that capacity fade is observed even for stoichio-

* Corresponding author. Tel.: +82-63-2702311; fax: +82-63-2702306.

E-mail address: nahmks@moak.chonbuk.ac.kr (K.S. Nahm).

0013-4686/01/$ - see front matter
PII: S0013-4686(00)00710-6

metrically synthesized $LiNiO_2$ due to the formation of the NiO_2 phase by the phase transition of the $LiNiO_2$ structure when charging up to a high voltage (> 4.0 V vs. Li^+/Li) during deintercalation of lithium ions.

An excess lithium method has been employed in a solid state reaction to synthesize a stoichiometric $LiNiO_2$ [8–10]. However, this method requires the removal of unreacted excess lithium by a washing step with deionised water. A sol–gel method has frequently been utilized to synthesize stoichiometric lithium metal oxides [11,12]. Meanwhile, the improvement of the cycle life of the $LiNiO_2$ electrode has extensively been attempted by substituting Ni in $LiNiO_2$ by some transition metals M to make $LiM_xNi_{1-x}O_2$ (M = Al, Co, Ga, Mg, Ti,…etc.) [13–18]. It has been reported that the substitution process stabilizes the crystal structure of the material during the intercalation/deintercalation of lithium ions even to produce the overcharged state, resulting in improvement of $LiNiO_2$ cyclability.

In this work, a sol–gel method was employed to prepare $LiNiO_2$. We have attempted to synthesize stoichiometric $LiNiO_2$ using a lithium excess method. Al-doped lithium nickel oxides were also prepared in the form of $LiAl_yNi_{1-y}O_2$ ($y = 0.0$, 0.1, 0.3) to alleviate the capacity fade of $LiNiO_2$. The structural and electrochemical properties of the prepared materials were characterized at room and high temperatures.

2. Experimental

Lithium excess $Li_{1+x}NiO_2$ ($x = 0.0$, 0.01, 0.02) and Al-doped $LiAl_yNi_{1-y}O_2$ ($y = 0$, 0.1, 0.3) powders were synthesized using a sol–gel method described in our previous work [19]. Lithium acetate ($Li(CH_3COO)\cdot 2H_2O$), aluminum nitrate ($Al(NO_3)_3\cdot 9H_2O$) and nickel acetate ($Ni(CH_3COO)_2\cdot 4H_2O$) salts were used as starting materials for the synthesis of $Li_{1+x}NiO_2$ and $LiAl_yNi_{1-y}O_2$ powders. For $LiNiO_2$, for example, stoichiometric amounts of Li ($Li(CH_3COO)\cdot 2H_2O$) and Ni acetate ($Ni(CH_3COO)_2\cdot 4H_2O$) salts (cationic ratio of Li:Ni = 1:1) were dissolved in deionised water. The dissolved solution was added drop by drop into a continuously agitated aqueous solution of adipic acid, the chelating agent for the reaction. The molar ratio of adipic acid to the total metal ions was unity. The pH of the solution was adjusted in the range of 2.5–3.5 by adding acetic acid. The prepared solution was evaporated at 70–80°C for 5 h until a transparent sol was obtained. As the water evaporated further, the sol turns into a viscous transparent gel. The resulting gel precursors were heated using the rate of 1°C min^{-1} and decomposed at 450°C for 10 h in air to eliminate organic components. The decomposed powders were calcined at 750°C in flowing oxygen for 14 h. The cooling rate of the powders was 1°C min^{-1} to prevent cation mixing in $LiNiO_2$.

After the synthesis, the amounts of Li, Ni, and Al in the synthesized materials were analyzed using inductively coupled plasma (ICP) to determine the real chemical composition of the materials. The oxygen content was determined via mass balance. Powder X-ray diffraction (XRD, D/Max-3A, Rigaku) measurements using Cu–Kα radiation was employed to characterize the structures of the synthesized powders. Particle morphology of the powders after calcination was observed using a scanning electron microscope (SEM, GEOL, JSM 6400). Rietveld refinement was performed with the XRD data to obtain lattice parameters of the synthesized powders. Quadrapole mass spectroscope (QMS, HAL2/511, HIDEN) was also used to analyze the gas evolved during the calcination of the as-prepared gel precursors.

The electrochemical characterization was performed using CR2032 coin-type cells. The method of assembling the cell was as follows: the cathode was fabricated using accurately weighed active material (20 mg) and a conductive binder (13 mg). It was pressed onto a 25 mm^2 stainless steel mesh used as the current collector at 300 kg cm^{-2} and dried at 200°C for 5 h in an oven. This cell consisted of a cathode and a lithium metal anode (Cyprus Foote Mineral Co.) separated by a porous polypropylene film as the separator (Celgard 3401). The electrolyte used was 1 M $LiPF_6$ in an ethylene carbonate (EC)/dimethyl carbonate (DMC) (v/v 1:2) solvent mixture. The cell was assembled in an argon-filled dry box and tested at room and high (50°C) temperatures. The cell was charged and discharged at a current density of 0.4 mA cm^{-2} (C/3) with cut-off voltages of 3.0 to 4.3 V (vs. Li/Li^+).

3. Results and discussion

3.1. Gas analysis during decomposition of gel precursor

In order to investigate the thermal properties of the synthesized gel precursors, the composition of the gas mixture produced during decomposition of the $LiNiO_2$ gel precursor was analyzed using a QMS. The QMS was operated at 10^{-5} torr at room temperature during the analysis. The synthesized precursor (0.5 g) was loaded into a sample holder in a tubular quartz reactor, heated by a tubular furnace. The temperature was monitored just below the sample holder and raised with a heating rate of 5°C min^{-1} using a PID (proportional-integral-derivative) controller. The outlet of the reactor was connected to the QMS using a quartz capillary tube (0.5 mm). In the connection, a two-stage-precision-needle-valve was used to overcome the pressure difference between the reactor and the QMS system.

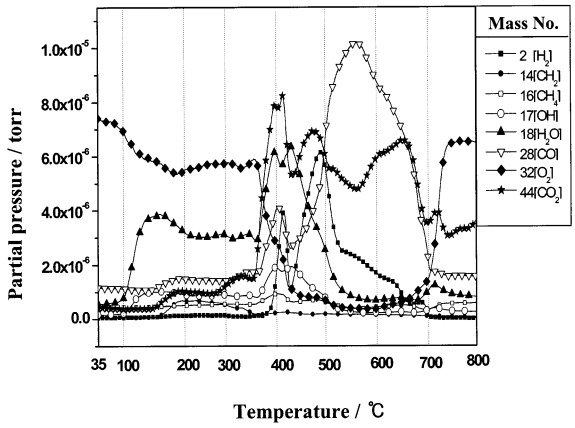

Fig. 1. Plots of partial pressures of gaseous species evolved from $LiNiO_2$ gel precursor during calcination as a function of decomposition temperature.

During analysis, the reactor was evacuated using a vacuum pump and oxygen was flowed through the reactor at 250 cm^3 min^{-1}.

Fig. 1 shows the partial pressures of gaseous species evolved during the decomposition of the gel precursor as a function of the temperature. It is observed that the moisture in the precursor begins to desorb at above 100°C. It seems that most of the starting materials used for the synthesis begin to decompose at about 400°C, which is consistent with the TGA and DTA analyses observed in our previous report [19]. The partial pressures of CO_2, H_2O, and H_2 gases greatly increase at around 400°C, whereas the partial pressure of CO is much smaller than that of CO_2. These evolved gases mainly originate from the decomposition of starting materials and chelating agents. It is interesting to see that the partial pressure of oxygen rapidly decreases from about 400°C and remains at a very low level in the temperature range from 400–700°C. At above 700°C, the partial pressure of oxygen recovers its original value and levels off as the temperature increases further. This indicates that most of the crystallization of $LiNiO_2$ occurs in the temperature range and the synthetic reaction is terminated at about 700°C.

The starting materials began to decompose at about 400°C to produce a gas mixture mainly consisted of CO_2 and H_2O. It is natural to see the production of CO_2 and H_2O from the starting materials in the presence of O_2 during the decomposition process. Meanwhile, it seems that the primary evolution of CO and CO_2 in the crystallization process is due to the oxidation of free-deposited carbon in the presence of oxygen. This experimental observation clearly demonstrates that oxygen plays an important role in the synthesis of highly crystallized $LiNiO_2$, as suggested in previous experimental work [20–22].

3.2. Preparation of $Li_{1+x}NiO_2$

The chemically analyzed compositions of the prepared samples are listed in Table 1 together with the calculated composition as well as their XRD data. The chemical analyses show that the real compositions of the synthesized $LiNiO_2$, $Li_{1.01}NiO_2$, and $Li_{1.02}NiO_2$ powders are $Li_{0.98}NiO_2$, $Li_{1.02}NiO_2$, and $Li_{1.03}NiO_2$, respectively. Fig. 2 shows XRD spectra for $Li_{1+x}NiO_2$ powders prepared by the excess method. Fig. 2(a) is an XRD pattern for undoped $LiNiO_2$, whereas (b) and (c) are XRD patterns for $Li_{1.01}NiO_2$, and $Li_{1.02}NiO_2$ powders, respectively. The XRD spectra shows that all the prepared samples have the typical $LiNiO_2$ layered structure with space group $R\bar{3}m$. No impurity-related peaks are observed from the XRD spectrum of $LiNiO_2$, but the XRD peaks of LiOH and Li_2CO_3 impurities appear at $2\Theta = 22$ and 30° for the $Li_{1.01}NiO_2$, and $Li_{1.02}NiO_2$ powders, although their magnitudes are very low. All the peaks appearing on the XRD patterns were identified with the characteristic peaks of $LiNiO_2$ reported in the X-ray powder data file of JCPDS as well as in previously reported work [20,23].

Shown in the upper inset in Fig. 2 are the integrated intensity ratios of (003)/(104) and (006)/(101) peaks of the XRD patterns. The increase of lithium content in $Li_{1+x}NiO_2$ decreases the integrated peak intensity ratio of (003)/(104) from 1.5 to 1.38, while increasing that of (006)/(101) from 0.185 to 0.227. Similar trends were observed in our previously reported data on $Li_{1+x}NiO_2$

Table 1
Lithium content and lattice constants measured by ICP and Rietveld analysis, respectively

Normal composition	Lattice constants		R_{exp}	R_{wp}	Measured lithium content
	a (Å)	c(Å)			
$Li_{1.00}NiO_2$	2.887	14.196	7.32	12.92	0.98
$Li_{1.01}NiO_2$	2.881	14.198	7.52	17.27	1.02
$Li_{1.02}NiO_2$	2.881	14.204	7.75	17.52	1.03
$LiAl_{0.1}Ni_{0.9}O_2$	2.869	14.210	12.35	27.25	1.00
$LiAl_{0.3}Ni_{0.7}O_2$	2.854	14.216	9.57	24.77	1.00

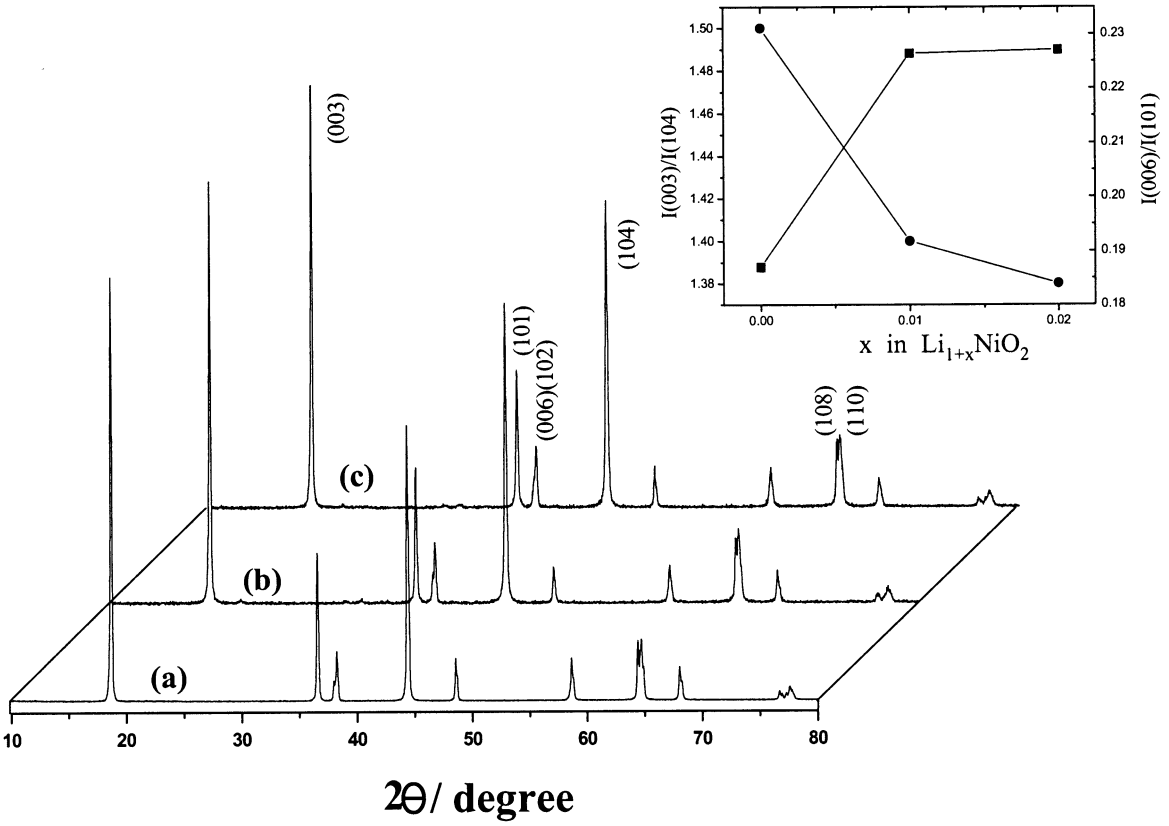

Fig. 2. X-ray diffraction patterns for $Li_{1+x}NiO_2$ powders prepared at various lithium contents. The gel precursors were calcined at 750°C in O_2. (a) $Li_{1.0}NiO_2$; (b) $Li_{1.01}NiO_2$; and (c) $Li_{1.02}NiO_2$. The upper inset showed the peak ratio of I(003)/I(104) and I(006)/I(101) as a function of lithium content.

($x = 0.03$ and 0.05) [19]. The (003) peak occurs from the diffraction of layered rocksalt structure $R\bar{3}m$, whereas the (104) peak appears from both the diffraction's of layered and cubic rocksalt structures [24]. Ohzuku et al. [23] evaluated the crystal quality of synthesized $LiNiO_2$ by measuring the integrated intensity ratio of (003) and (104) peaks and reported that the decrease of the (003)/(104) peak intensity ratio indicates the formation of the cubic $LiNiO_2$ structure due to the displacement of nickel and lithium ions. Meanwhile, Nitta et al. [25] also proposed that the integrated intensity ratio of the (006) and (101) peaks should be less than 1.0 in order to obtain better electrochemical properties from the synthesized $LiNiO_2$. The upper inset in Fig. 2 shows that the values of the (003)/(104) and (006)/(101) peak ratios drastically vary with the initial value of x, in the range 0–0.01, but thereafter only slightly with further addition of lithium. According to the above literature [24,25], it is considered that the excess amount of lithium ($x = 0.01$ and 0.02) might increase the formation of cubic phase in the host material, resulting in a degradation of electrode performance.

The lattice constants, a and c, of $Li_{1+x}NiO_2$ were calculated by the Rietveld refinement method using the XRD data and are presented in Table 1 as a function of the x value with the other analytic data. As the x value increases, the lattice constant a decreases very slightly from 2.889 to 2.885 Å, whereas the lattice constant c increases slightly from 14.198 to 14.205 Å. The increasing lithium content in $Li_{1+x}NiO_2$ ($x > 0$) reduces the oxidation state of nickel from Ni^{3+} to Ni^{2+}. This might cause the elongation of c-axis because the ionic size of Ni^{2+} (0.83 Å) is larger than that of Ni^{3+} (0.70 Å) [20].

3.3. Preparation of $LiAl_yNi_{1-y}O_2$

In order to improve the electrochemical properties of $LiNiO_2$, nickel ions were partially substituted by aluminum ions. The chemically analyzed compositions of the Al-doped samples were $LiAl_{0.1}Ni_{0.9}O_2$ and $LiAl_{0.3}Ni_{0.7}O_2$, respectively, as presented in Table 1. Fig. 3 presents XRD patterns of $LiAl_{0.1}Ni_{0.9}O_2$ and $LiAl_{0.3}Ni_{0.7}O_2$ as well as of $LiNiO_2$ for comparison. The figure shows that almost similar XRD patterns are

observed for all the Al-doped samples without the inclusion of any other impurities. As the aluminum content increases, however, the (006) peak shifts towards lower diffraction angles and the (110) peak shifts towards higher diffraction angles. The transition of these diffraction angles results in a clear split of the (006)(102) and the (108)(110) lines of $LiNiO_2$. In addition, it is observed that the (110) and (113) peaks broaden as the aluminum content increases in $LiAl_yNi_{1-y}O_2$. Similar phenomena have already been reported in the previously reported literature [26], which explained that the above observations were because the aluminum ion substituted into the nickel site generates a microscopic stress in the basal plane of $LiNiO_2$. The lattice constants, *a* and *c*, of $LiAl_{0.1}Ni_{0.9}O_2$ and $LiAl_{0.3}Ni_{0.7}O_2$ were calculated by the Rietveld refinement using the XRD data of Fig. 3 and are summarized in Table 1 with their chemical compositions. As the aluminum content increases, the lattice constant *a* decreases from 2.889 for $LiNiO_2$ to 2.885 Å for $LiAl_{0.3}Ni_{0.7}O_2$, whereas *c* increases from 14.197 for $LiNiO_2$ to 14.215 Å for $LiAl_{0.3}Ni_{0.7}O_2$. Such an anisotropic change in the lattice constants, *a* and *c*, is a typical characteristic of a layered structure. Ohzuku et al. [26] reported that the substitution of nickel ions in $LiNiO_2$ by aluminum ions results in the *a*-axis shortening and the *c*-axis enlarging as the lithium amount increases up to 0.25, after which these parameters level off.

Fig. 4(a) and (b) show SEM photographs for $LiNiO_2$ and $LiAl_{0.1}Ni_{0.9}O_2$ powders, respectively. The average particle sizes are about 0.2–0.6 μm for $LiNiO_2$ and 0.1–0.4 μm for $LiAl_{0.1}Ni_{0.9}O_2$. It is considered that the crystallite size of $LiAl_yNi_{1-y}O_2$ decreases with the substituted amount of aluminum ions because the diffusion rate of the aluminum into the $LiNiO_2$ system is so slow that it retards the growth of the particles at the same temperature as the $LiNiO_2$ grows. The upper inset in Fig. 3 shows the crystallite size of $LiAl_yNi_{1-y}O_2$ versus the substituted amount of aluminum ions. The

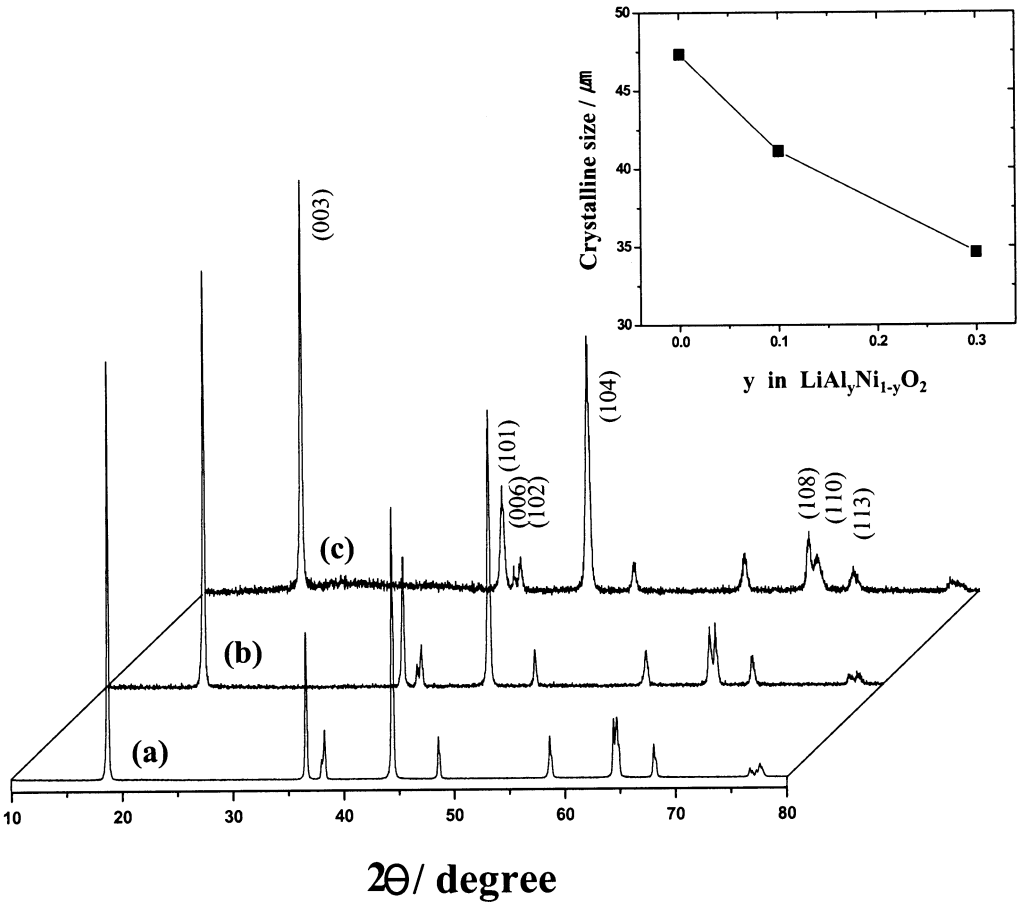

Fig. 3. X-ray diffraction patterns for $LiAl_yNi_{1-y}O_2$ powders prepared at various aluminum contents. The gel precursors were calcined at 750°C in O_2. (a) $Li_{1.0}NiO_2$; (b) $LiAl_{0.1}Ni_{0.9}O_2$; and (c) $LiAl_{0.3}Ni_{0.7}O_2$. The upper inset showed the crystallite size as a function of aluminum content.

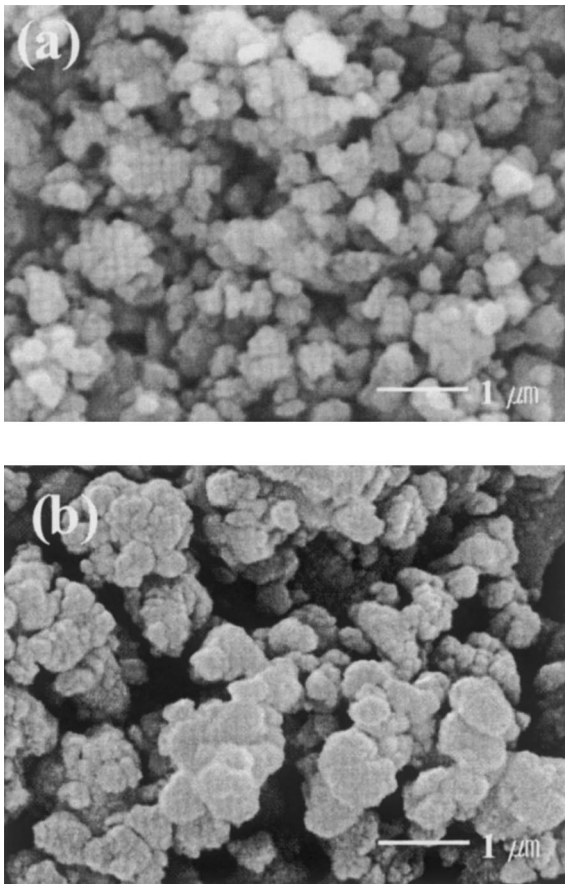

Fig. 4. Scanning electron micrographs for (a) $LiNiO_2$ and (b) $LiAl_{0.1}Ni_{0.9}O_2$.

crystallite size was calculated by applying the values of full width half maximum (FWHM) of the (003) peaks in Fig. 3 to the Scherrer equation [27]. The figure shows that the crystallite size of $LiAl_yNi_{1-y}O_2$ decreases with the increase in the substituted amount of aluminum ions, indicating the increase of the FWHM of the (003) peak. In a recent paper, it has been reported that the increase of the (003) peak width is attributed to a decrease in the crystallite size of $LiNiO_2$ particles and/or to an increase in the homogeneous strain in the particles during the reaction [28]. The increase of the FWHM of the (003) peak indicates the deterioration of $LiNiO_2$ crystal quality. From the XRD data for the Al-doped samples, however, it seems that the crystallite size of the $LiNiO_2$ particles is influenced by the addition of aluminum ions rather than by the $LiNiO_2$ crystal quality.

3.4. Electrochemical properties of synthesized materials

Fig. 5 shows plots of the discharge capacity measured at room temperature as a function of the cycle number for the Li/$LiPF_6$–EC/DMC (v/v 1:2)/$Li_{1+x}NiO_2$ (and $LiAl_yNi_{1-y}O_2$) cells fabricated using the synthesized $Li_{1+x}NiO_2$ ($x=0$–0.02) and $LiAl_yNi_{1-y}O_2$ ($y=0$–0.3), respectively. The cells were tested under a constant charge/discharge current density of 0.4 mA cm^{-2} (C/3) between 3.0 and 4.3 V. The initial discharge capacities of $LiNiO_2$, $Li_{1.01}NiO_2$, and $Li_{1.02}NiO_2$ are 160, 142, and 141 mAh g^{-1}, respectively. But the capacity slowly decreases with the cycle number to 130, 112, and 107 mAh g^{-1} after the 50th cycle for the corresponding materials, respectively.

The inset in Fig. 2 showed the decrease of the integrated intensity ratio of the (003)/(104) peaks with the increase of lithium content in $Li_{1+x}NiO_2$. It is likely that the excess amount of lithium ($x=0.01$ and 0.02) slightly affects the degree of the displacement of nickel and lithium ions in the lithium nickel oxides, resulting in the degradation of battery performance, although all the prepared samples have a typical $R\bar{3}m$ structure. It is also considered that the increase of lithium content in $Li_{1+x}NiO_2$ decreases the oxidation state of some Ni ions from Ni^{3+} to Ni^{2+}, which might increase the formation of an electrochemically inert phase in the $LiNiO_2$ host material since Ni^{2+} has a more stable state [29]. This may impede the motion of the lithium ions leading to the deterioration of the electrode during the charge and discharge. Yamada et al. measured the initial discharge capacity as a function of average oxidation state of Ni in $LiNiO_2$ material [20]. They observed that the initial discharge capacity was the highest when the oxidation state of nickel ion

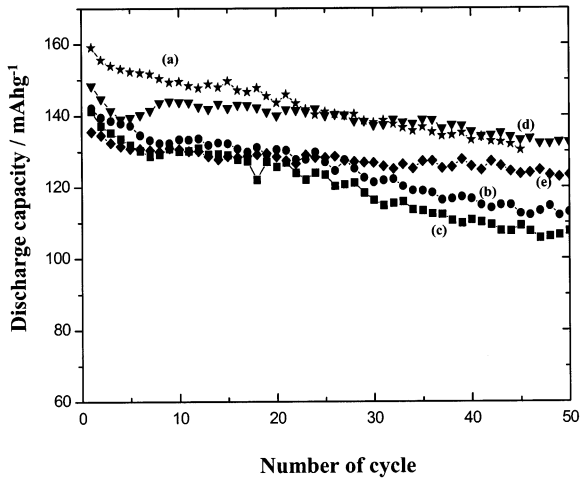

Fig. 5. Plots of specific discharge capacity versus number of cycles for the Li/$LiPF_6$–EC/DMC(v/v 1:2)/$Li_{1+x}NiO_2$ (and $LiAl_yNi_{1-y}O_2$) powders calcined at 750°C in O_2. Cycling was carried out galvanostatically at constant charge–discharge current density of 0.4 mA cm^{-2} between 3.0–4.3 V at room temperature: (a) $Li_{1.0}NiO_2$; (b) $Li_{1.01}NiO_2$; (c) $Li_{1.02}NiO_2$; (d) $Li_{1.0}Al_{0.1}Ni_{0.9}O_2$; and (e) $Li_{1.0}Al_{0.3}Ni_{0.7}O_2$.

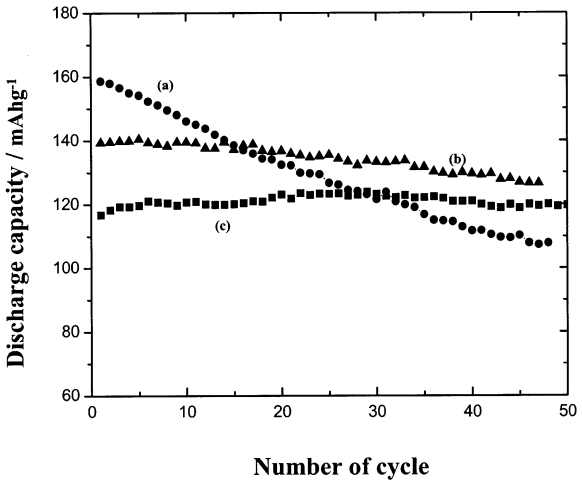

Fig. 6. Plots of specific discharge capacity versus number of cycles for the Li/$LiPF_6$–EC/DMC(v/v 1:2)/$LiAl_yNi_{1-y}O_2$ powders calcined at 750°C in O_2. Cycling was carried out galvanostatically at constant charge–discharge current density of 0.4 mA cm^{-2} between 3.0–4.3 V at high temperature (50°C). (a) $Li_{1.0}NiO_2$; (b) $Li_{1.0}Al_{0.1}Ni_{0.9}O_2$; and (c) $Li_{1.0}Al_{0.3}Ni_{0.7}O_2$.

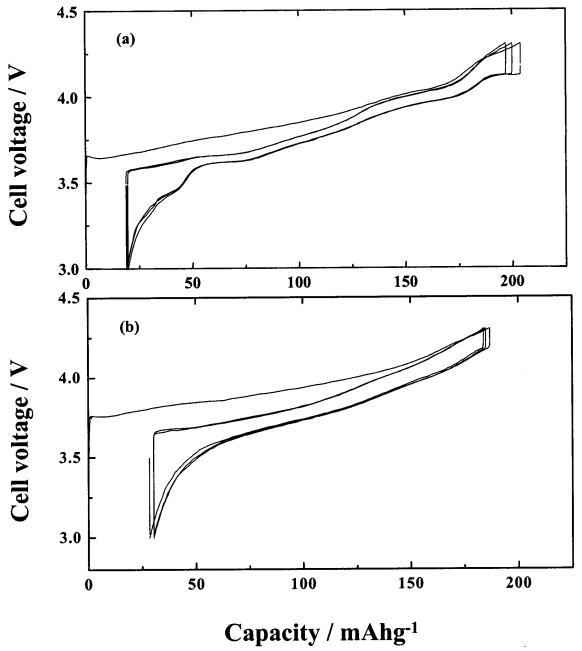

Fig. 7. Charge–discharge curves for (a) $LiNiO_2$ and $LiAl_{0.1}Ni_{0.9}O_2$ measured at 50°C.

was 3.0, corresponding to the high crystal quality of $LiNiO_2$. It also seems that the decrease of the initial discharge capacity is due to the formation of LiOH and Li_2CO_3 impurities in the $LiNiO_2$ host material, as seen in Fig. 2.

The capacity fade of $Li_{1+x}NiO_2$ is considered to be due to the destruction of the NiO_2 layer in the $LiNiO_2$ crystal lattice by the extraction of lithium ions during the charging process, as observed from the structural analysis of $LiNiO_2$ by Li et al. [30]. During the charging process, they observed that $LiNiO_2$ shows sequential change in crystal structure from the hexagonal phase to the monoclinic phase, the hexagonal phase again, then two hexagonal phases, and finally to a single hexagonal phase. The second hexagonal phase that has appeared in the two regions causes the sudden shrinkage of the crystal lattice because of its small c-lattice parameter. They suggested that this seems to be related to the deformation of the NiO_2 layer in the $LiNiO_2$ crystal lattice, and such deformation may result in an irreversible structure change.

However, the capacity retention rates of the cells are significantly improved for the Li/$LiPF_6$–EC/DMC(v/v 1:2)/$LiAl_yNi_{1-y}O_2$ cells, although the initial capacity of the cells decreases with increasing Al content in $LiAl_yNi_{1-y}O_2$. The substitution of aluminum ions for nickel ions for $LiNiO_2$ is possible because $LiAlO_2$ is iso-structural with $LiNiO_2$ [31]. In the overcharged state of $LiNiO_2$, most of the Ni ions are in the unstable Ni^{4+} state, which leads to the capacity fade by the mixing of lithium and nickel ions. However, when nickel ions are substituted with aluminum ions, the amount of lithium ions, which can be (de) or intercalated would be limited because aluminum ions remain in an oxidation state of +3. This results in the decrease of the initial capacity of Al-doped $LiNiO_2$. Some other researchers have also observed that the initial capacity of the $LiAl_yNi_{1-y}O_2$ cell is significantly reduced with the increase of Al content in $LiAl_yNi_{1-y}O_2$ [26,32]. On the other hand, the doped aluminum ion enhances the stability of $LiNiO_2$ structure because the bonding energy of Al–O (512 kJ mol^{-1}) is higher than that of Ni–O (391.6 kJ mol^{-1}) [33].

Fig. 6 shows a plot of the discharge capacity measured at 50°C as a function of the cycle number for the Li/$LiPF_6$–EC/DMC(v/v 1:2)/$LiAl_yNi_{1-y}O_2$ ($y = 0$–0.3) cells. For the $LiNiO_2$ cell, the initial capacity is about 160 mA g^{-1}, but the capacity fade of the cell is much faster at 50°C than at room temperature Meanwhile, Al-doped $LiAl_yNi_{1-y}O_2$ cells deliver lower initial discharge capacities, but the capacity fade of the cells is very small and negligible. In other words, the $LiAl_yNi_{1-y}O_2$ system shows an excellent cycle performance at high temperature but not at room temperature This behavior can clearly be explained using the charge–discharge curves for $LiNiO_2$ and $LiAl_{0.1}Ni_{0.9}O_2$ cells measured at 50°C, which are pictured in Fig. 7 (a) and (b), respectively. Fig. 7 shows that the charge–discharge curve of $LiAl_{0.1}Ni_{0.9}O_2$ (Fig. 7(b)) is quite different from that of $LiNiO_2$ (Fig. 7(b)). The charge–discharge curve of $LiNiO_2$ at high temperature (Fig. 7(a)) has four distinct plateaux in the whole cut-off voltage region. The plot agrees well with results

published in the literature, which show four-stepped structural changes in the charge process [29,30]. The appearance of the potential plateau near 4.0 V Li/Li^+ is due to the formation of NiO_2 phase, which causes the capacity fade of the $LiNiO_2$ electrode with cycle number. However, the plateau is not observed in the charge–discharge curves of $LiAl_{0.1}Ni_{0.9}O_2$ at 50°C (Fig. 7(b)). The observation of monotonous curves in the overcharge voltage region indicates that no phase transition occurs and lithium ion diffusion proceeds in a single phase. The doped aluminum ion of the $LiAl_{0.1}Ni_{0.9}O_2$ material enhances the stability of the $LiNiO_2$ structure and helps to maintain the layered structure in the charge–discharge process. This is why the cyclability of $LiAl_yNi_{1-y}O_2$ ($y = 0.1$ and 0.3) is superior to that of $LiNiO_2$ at the high temperature.

4. Conclusions

$Li_{1+x}NiO_2$ ($x = 0$–0.02) and $LiAl_yNi_{1-y}O_2$ ($y = 0$–0.3) powders were synthesized by a sol–gel method using adipic acid as a chelating agent. Analysis of gas evolved from the $LiNiO_2$ gel precursor during calcination showed that most of the starting materials used for the synthesis decomposed at about 400°C and the partial pressure of oxygen rapidly decreased from about 400°C and remained only very low in the temperature range where most of the crystallization occurred. $Li_{1+x}NiO_2$ powders prepared by the excess lithium method had a typical $R\bar{3}m$ structure. The initial capacity of the cells fabricated using $Li_{1+x}NiO_2$ decreased as the lithium content increased. But the discharge capacity slowly decreased with the cycle number. Meanwhile, the room temperature capacity retention rate of the cells fabricated using $LiAl_yNi_{1-y}O_2$ were significantly improved although the initial capacity of the cells decreased with an increase of the Al content in $LiAl_yNi_{1-y}O_2$. Furthermore the capacity fade of this cell at high temperature (50°C) was almost negligible. The Al-doped $LiNiO_2$ cathode material was very effective to increase cycle performance of $LiNiO_2$ cells at high temperature.

Acknowledgements

The authors wish to acknowledge the financial support of the Korea Research Foundation made in the program year of (1998).

References

[1] K. Mizushima, P.C. Jones, P.J. Wiseman, J.B. Goodenough, Mater. Res. Bull. 15 (1980) 783.
[2] C. Plichta, M. Salomon, S. Slane, M. Uchiyoma, B. Chua, W.B. Ebner, H.W. Lin, J. Power Sources 21 (1987) 25.
[3] J.R. Dahn, U. Von Sacken, C.A. Michel, Solid State Ionics 44 (1990) 87.
[4] C. Delmas, Mater. Sci. Eng. B3 (1989) 97.
[5] A.F. Wells, Structual Inorganic Chemistry, fifth edition, Oxford Science, London, p.577.
[6] J.N. Reimers, W. Li, E. Rossen, J.R. Dahn, in: G.A. Nazri, J.M. Tarascon, M. Armand (Eds.), MRS Symposium Proceedings, vol. 293, MRS, Pittsburg, 1993, p. 3.
[7] T. Ohzuku, H. Komori, M. Nagayama, K. Sawai, T. Hirai, Chem. Express. 6 (1991) 161.
[8] H. Arai, S. Okada, H. Ohtsuka, M. Ichimura, J. Yamaki, Soild State Ionics 80 (1995) 261.
[9] H. Arai, S. Okada, Y. Sakurai, J. Yamaki, J. Electrochem. Soc. 144 (1997) 3117.
[10] H. Arai, S. Okada, Y. Sakurai, J. Yamaki, Solid State Ionics 109 (1998) 295.
[11] S. Bach, M. Henry, N. Battier, J. Livage, J. Solid State Chem. 88 (1990) 325.
[12] J.P. Pereira-Ramos, R. Baddour, S. Bach, N. Baffier, Solid State Ionics 80 (1992) 701.
[13] T. Ohzuku, T. Yanagawa, M. Kouguchi, A. Ueda, J. Power Sources 68 (1997) 131.
[14] Y. Nitta, K. Okamura, K. Haraguchi, S. Kobayashi, A. Ohta, J. Power Sources 54 (1995) 511.
[15] B. Banov, J. Bourilkov, M. Mladenov, J. Power Sources 54 (1995) 268.
[16] Y. Nishida, K. Nakane, T. Satoh, J. Power Sources 68 (1997) 561.
[17] H. Arai, S. Okada, Y. Sakurai, J. Yamaki, J. Electrochem. Soc. 144 (1997) 3117.
[18] Y. Gao, M.V. Yakovleva, W.B. Ebner, Electrochem. Solid State Lett. 1 (1998) 117.
[19] Y.S. Lee, Y.K. Sun, K.S. Nahm, Solid State Ionics 118 (1999) 159.
[20] S. Yamada, M. Fujiwara, M. Kanda, J. Power Sources 54 (1995) 209.
[21] G.X. Wang, S. Zhong, D.H. Bradhurst, S.X. Dou, H.K. Liu, J. Power Sources 76 (1998) 141.
[22] M. Okada, K. Takahashi, T. Mouri, J. Power Sources 68 (1997) 545.
[23] T. Ohzuku, A. Ueda, M. Nagayama, J. Electrochem. Soc. 140 (1993) 1862.
[24] J. Morales, C. Peres-Vicente, J.L. Tirado, Mat. Res. Bull. 25 (1990) 623.
[25] Y. Nitta, K. Okamura, K. Haraguchi, S. Kobayashi, A. Ohta, J. Power Source 54 (1995) 511.
[26] T. Ohzuku, A. Ueda, M. Kouguchi, J. Electrochem. Soc. 142 (1995) 4033.
[27] H.P. Klug, L.E. Alexander, X-ray Diffraction Procedure for Polycrystalline and Amorphous Materials, second ed., Wiley, New York, 1974.
[28] M.R. Polacin, D. Larcher, A. Audemer, N. Sac-Epec, G.G. Amatucci, J.M. Tarascon, J. Electrochem. Soc. 144 (1997) 4226.
[29] K. Kubo, M. Fujiwara, S. Yamada, S. Arai, J. Power Sources 68 (1997) 553.
[30] W. Li, J.N. Reimers, J.R. Dahn, Solid State Ionics 67 (1993) 123.
[31] A.M. Lejus, R. Collongues, C. R. 254 (1962) 2005.
[32] Q. Zhong, U. Sacken, J. Power Sources 54 (1995) 221.
[33] J.A Dean, Lange's Handbook of chemistry, fourth ed., McGraw-Hill, New York, 1992, p. 4.